Molecular dynamics simulation of surface nucleation during growth of an alkane crystal

Alexander Bourque[a], C. Rebecca Locker[b], Gregory C. Rutledge[a*]

[a]Department of Chemical Engineering, Massachusetts Institute of Technology, Cambridge, MA 02139

[b]ExxonMobil Research and Engineering Company, Annandale NJ 08801

[*]Corresponding author. Tel.: +1 617 253 0171; fax: +1 617 258 5766.

E-mail address: rutledge@mit.edu (G. C. Rutledge).

1. Abstract

Crystal growth from the melt of n-pentacontane (C50) was studied by molecular dynamics simulation. Quenching below the melting temperature gives rise to propagation of the crystal growth front into the C50 melt from a crystalline polyethylene surface. By tracking the location of the crystal-melt interface, crystal growth rates between 0.02-0.05 m/s were observed, for quench depths of 10-70 K below the melting point. These growth rates compare favorably with those from a previous study by Waheed et al (2005). Next, surface nucleation was identified with the formation of two-dimensional clusters of crystalline sites within layers parallel to the propagating growth front. Critical nucleus sizes, waiting times and rates for surface nucleation were estimated by a mean first passage time analysis. A surface nucleation rate of ~0.05 $nm^{-2}ns^{-1}$ was observed, and it was nearly temperature-independent. Post-critical "spreading" of the surface nuclei to form a completely crystallized layer slowed with deeper supercooling.

for Table of Contents use only

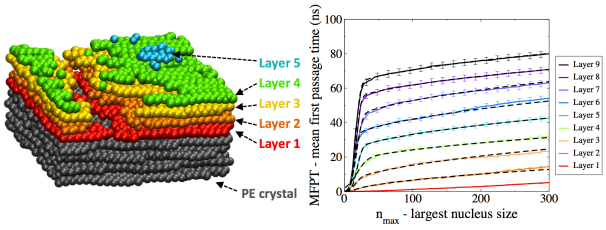

"Molecular dynamics simulation of surface nucleation during growth of an alkane crystal"

Alexander Bourque, C. Rebecca Locker, Gregory C. Rutledge

2. Introduction

Crystallization from polymer melts has numerous practical applications[1,2] and is a crucial step in the manufacturing of the vast majority of commodity and many specialty plastics. Of long-standing interest is the development of morphological structure during the transition from an initial, fully amorphous state to the semicrystalline state.[3,4] The microstructure in a semicrystalline polymer material ultimately determines its material properties, including bulk strength, impact resistance, and stiffness.[5] The characteristic microstructural feature of many crystallized polymer materials is the spherulite, a 3-dimensional, radially symmetric arrangement of stacked crystalline lamellae interspersed by regions of amorphous polymer. Despite the abundance of research into the structure of the spherulite and its evolution during crystallization,[4,6,7,8,9] a clear description of its development remains elusive.[10] Refined models for lamellar crystal growth within spherulites and other microstructures would greatly improve the ability to predict morphological structure and target the evolution of novel morphologies for enhanced material properties.

Lauritzen and Hoffman (LH) first proposed the concept of surface nucleation[11] to explain the growth of the lamellar polymer crystals.[12,13] According to LH theory, propagation of the crystal growth front proceeds in two steps: (1) an activated surface nucleation event, characterized by a crystalline stem depositing on the leading edge of the crystal growth front, and (2) lateral spreading of the surface nucleus through the addition of crystalline stems to complete a crystalline layer of the growing lamella. LH theory is supported by experimental results that indicate the lamellar thickness obtained during isothermal crystallization increases with crystallization temperature T_c (i.e. shallower supercooling, $\Delta T=T_m-T_c$), and by the existence of three distinct regimes of temperature-dependent growth[14] represented schematically in Figure 1. LH argued that the regimes were consistent with surface nucleation, arising out of a competition between relative rates for the initial deposition of a crystalline stem (i.e. surface nucleation) and subsequent spreading of the crystal across the surface by the addition of more stems. LH theory has been widely applied to interpret the rate of crystal growth in numerous common polymers such as PE,[15] PEO[16]

and i-PP.[17] Growth rates in these polymer systems have been observed to exhibit all three regimes of growth.

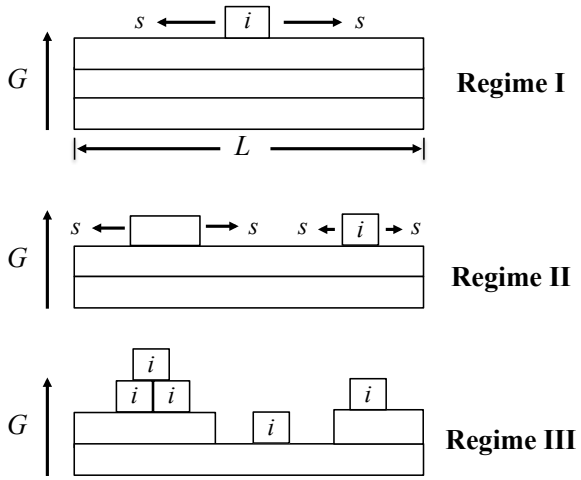

Figure 1. Growth rate *G* on the surface of a lamella as envisioned in the classical theory proposed by Lauritzen and Hoffman. Lamellae are represented looking down the molecular chain axis of deposited stems. Stem deposition occurs at a rate *i* on an available surface. Additional stems add to the nucleus, spreading at a rate *s*. Competition among *s* and *i* result in three distinct regimes of growth.

However, LH theory is not without its critics. Since its inception, much debate has surrounded the mechanism of molecular attachment during nucleation and subsequent lateral spreading, and the consequences of such mechanisms. LH theory assumes that a fully-extended segment of the chain equal to the lamellar thickness serves as the critical nucleus, and subsequent stems attach also as fully-extended segments. Below a critical lamellar thickness l_{min}, the attachment of subsequent stems results in a net increase in free energy and an unstable lamella. In the LH theory, the observed lamellar thickness l^* is that which grows fastest and therefore dominates crystallization. Frank and Tosi proposed a variant of LH theory that allows for deposition of the stem via single repeat unit attachment (or detachment) stages.[18] The length of the crystal stem increases with deposition of additional repeat units until it reaches the observed lamellar thickness, at which point a fold is introduced, and repeat unit addition continues into

the next stem. Point proposed a model that allows for repeat unit attachment/detachment and folding at any point during the deposition of the initial stem;[19] in his model, subsequent stems attach as one unit, with a stem length equal to the initial nucleated stem. Detachment of subsequent stems can also take place, allowing the nucleus to grow or shrink and thereby change the lamellar thickness. Point's model addressed a shortcoming of LH theory in which an infinite lamellar thickness was predicted at very deep supercoolings. For further information regarding the extensive history of polymer crystallization theories, the review by Armistead and Goldbeck-Wood is recommended.[20]

In contrast to LH theory, others have proposed models that do not rely on an enthalpic surface nucleation barrier for crystal growth. Sadler and Gilmer proposed an entropic barrier model[21] based upon kinetic Monte Carlo simulations of polymer crystallization. In their model, the growth face explores many configurations, only a small fraction of which result in successful propagation of the growth front. Using a more sophisticated kinetic Monte Carlo model that incorporated free energy costs for the polymer to extend beyond the edges of the previous crystalline layer as well as for a stem to be shorter than l_{min}, Doye and Frenkel concluded that lamellar propagation would converge towards growth with constant thickness.[22] Binsbergen has also challenged the strict requirements of the surface nucleus, adding that the LH theory ignores alternative pathways with lower energy barriers to creating a new layer.[23] Like Sadler and Gilmer, Binsbergen stressed the stochastic nature of crystal growth.

More recent models have argued for intermediate stages during crystal growth. For example, Keller and co-workers showed that crystal growth in PE could proceed with the formation first of a hexagonal phase at short stem length, which then transition to a more stable orthorhombic phase as the lamella thickens.[24,25] Strobl also proposed a multi-step mechanism for lamellar crystallization.[26] In his model, the initial step is the formation of a "mesomorphic" layer on the lateral growth face. Essentially, chain sequences attach without completely ordering, such that the density of this initial layer is slightly greater than that of the melt. When this mesomorphic layer reaches a critical thickness in the growth direction, it solidifies through a cooperative structural transition. The result is a series of "granular crystals", preceded

by a roughly ordered, mesomorphic layer. In the final step, granular crystals merge to form the characteristic lamellar structure. The evidence supported by the models of Keller and Strobl is consistent with "two-step nucleation" models that have become prevalent in other areas of crystallization study.[27,28,29]

Despite these numerous efforts, however, none of the foregoing models is capable of describing polymer crystallization using parameters that can be derived solely from chemical architecture and first principles. All rely to some degree on empirical parameterization. The experimental evidence is obtained in the form of macroscopic growth rates and inferences based upon crystalline lamellar thickness. It remains unclear what molecular processes are occurring at the crystal growth front or exactly what the critical nucleation event looks like, since current experimental techniques are incapable of such fine spatiotemporal resolution. These limitations have prompted the pursuit of alternative routes toward the investigation of polymer crystallization. Molecular simulation provides an invaluable alternative for the study of polymer crystallization from the solution or melt. Most importantly, one can observe nucleation,[30,31,32] lateral spreading[33] and propagation of the growth front[34,35,36] separately through careful selection of simulation conditions and appropriate data analyses.

Crystal growth of $C_{20}H_{42}$,[35] $C_{50}H_{102}$ and $C_{100}H_{202}$[33] was previously examined using molecular dynamics simulations in a series of papers by Waheed and Rutledge. In that work, the crystal surface was modeled using a corrugated potential that mimicked the parallel alignment of stems, and crystal growth rates were measured by tracking the midpoint in an orientational order profile that varied from almost unity (for the crystal phase) to zero (for the amorphous melt phase). Molecular ordering within layers normal to the surface was analyzed through snapshots of the system. Evidence obtained from these simulations supported the formation of a small surface nucleus as part of the growth mechanism. However, the simulated spatial scale was too small to prevent early onset of finite size effects during layer ordering, prohibiting a deeper analysis of surface nucleation phenomena. Additionally, the analysis of surface

ordering was only conducted in the three layers closest to the artificial, rigid surface, so artifacts could have been significant.

In this study, we rectify the shortcomings of Waheed and Rutledge, and extend our analysis to the quantitative description of surface nucleation and spreading mechanisms. The analysis performed in this work draws upon the techniques used by Yi and Rutledge in studies of primary nucleation of alkanes from the homogeneous melt. [32,37,38] A two-dimensional analogue of the mean first passage time concept previously employed in three dimensions to study primary nucleation is applied here to study the mechanism of nucleation on a surface at the leading edge of a crystal growth front. Surface nucleation and lateral spreading are examined layer by layer, to characterize the mechanism of crystal growth.

3. Theory

In classical nucleation theory, as it applies to primary nucleation, the rate of nucleation is the number of successful nucleation events arising per unit volume per unit time, and is expressed as the inverse of sample volume and a characteristic induction time. By analogy, the notion of surface nucleation implies that there exists a surface with area A upon which a nucleus of crystallizable material develops, with a characteristic induction time τ_n. The rate at which such nuclei develop is the surface nucleation rate i,

$$i = \frac{1}{\tau_n A} \tag{1}$$

According to transition state theory, the surface nucleation rate i is given by,

$$i = i_0 \exp\left(-\beta E_d\right)\exp\left(-\beta \Delta G^*\right) \tag{2}$$

where E_d is the activation energy for chain diffusion to (or perhaps across) the surface, ΔG^* is the free energy barrier to the formation of a critical surface nucleus, and i_o is a prefactor that is only weakly temperature-dependent. $\beta=1/k_BT$, where k_B is Boltzmann's constant.

According to LH theory, the surface nucleus develops as a single, atomic layer of chains. Single-stem clusters spontaneously attach at the leading edge of a growing lamella and spread to form a full molecular layer of crystallized material. Consistent with LH theory, we adopt here the notion of a surface nucleus as a pseudo two-dimensional cluster of crystallized material that is approximately one molecule thick, developing at the growth front; however, extending the analysis to clusters and layers that are two or more molecules thick, such as the "cylindrical cap" used by Howard and Milner[39], should be straightforward.

To characterize the surface nucleation event, a mean first passage time (MFPT) analysis is applied to the largest cluster n_{max} observed on a surface. As shown by Wedekind et al. for homogeneous nucleation,[40] the MFPT of the largest cluster size in a system, $\tau(n_{max})$, takes the form of the first term on the right hand side (rhs) of Eq. (3), as long as the critical free energy barrier is large relative to the thermal energy ($\Delta G^* >> k_B T$), and the subsequent growth (or spreading) of the nucleus is very much faster than the nucleation rate:

$$\tau(n_{\max}) = \tfrac{1}{2}\tau^* \left\{1 + erf\left[Z\sqrt{\pi}\left(n_{\max} - n^*\right)\right]\right\} + \tau_s\left(n_{\max}\right) H\left(\Delta n\right) \tag{3}$$

where τ^* is the waiting time, n^* is the critical nucleus size, and

$$Z = \sqrt{\frac{\beta}{2\pi}\left|\frac{d^2 G(n)}{dn^2}\right|} \tag{4}$$

is the Zeldovich factor, which is related to the local curvature at the height of the nucleation free energy barrier. Note that we distinguish between the *induction* time τ_n, which characterizes the likelihood of nucleation on an existing surface of crystallized area A, and the *waiting* time τ^*, which includes additionally the time required for the crystal growth front to propagate to the layer where n_{max} is measured.

To account for cases where the subsequent growth (or spreading) rate of the cluster is not much faster than the rate of nucleation itself, Yi et al. added the second term on the rhs of Eq. (3), of the form $\Delta\tau$ =

$\tau_s(n_{max})H(\Delta n)$, that triggers once the critical nucleus size is reached; $H(x)$ is the Heaviside function, and $\Delta n = n_{max} - n^*$ is the extent of supercriticality. They employed this modified equation to analyze MFPT data for homogeneous, primary nucleation in long chains (C150 and higher), for which the rate of nucleation was found to be on the same order of magnitude as the rate of growth. [32,37,38] Surface nucleation in n-alkanes experiences a similar issue, so we employ a similar ad hoc correction in this work.

The particular form of the spreading function $\tau_s(n_{max})$ is determined by the shape evolution of the nucleus. In general, one can write:

$$\tau_s\left(n_{\max}\right) = \frac{b}{s}\left[\frac{n_{\max}^{\alpha} - \left(n^*\right)^{\alpha}}{\left(h\rho_n\right)^{\alpha}}\right] \tag{5}$$

where s is the spreading rate, h is the thickness of the layer and ρ_n is the number density of sites in the crystalline material. b and α are parameters that depend on nucleus shape. In LH theory, where the surface nucleus comprises a single, fully extended stem and spreading proceeds by the subsequent deposition of adjacent, full length stems, $b = \alpha = 1$. For a circular, disk-like nucleus that grows with a constant, isotropic radial spreading rate, $b = (2\pi^{1/2})^{-1}$ and $\alpha = 1/2$.

According to the surface nucleation mechanism, propagation of the growth front into the melt proceeds layer by layer, with each crystalline layer nucleating and spreading on the layer before it, in a self-similar manner. Therefore, for a given layer k, the substrate surface is considered to be the crystallized area in the previous layer $k - 1$. Eq. (1) can thus be applied to calculate the surface nucleation rate i in layer k, given τ_n and the crystallized area of the substrate layer A_{k-1}. A defining feature of this problem is that A_{k-1} is not constant, but continues to increase during the nucleation induction period for layer k, due to spreading and/or additional surface nucleation events. The dynamic nature of the substrate area must be taken into account. We do this here by integrating the area A_{k-1} over the induction period for layer k. The time window of interest begins when the $k - 1^{th}$ layer nucleates (waiting time τ_{k-1}^*) and concludes when the k^{th}

layer nucleates (waiting time τ_k^*). The following expression is then used in lieu of Eq. (1) to evaluate the surface nucleation rate i_k for layer k,

$$i_k = \frac{1}{\int_{\tau_{k-1}^*}^{\tau_k^*} A_{k-1}(t)\,dt} \tag{6}$$

4. Simulation Method

Alkane chains were modeled with a united atom force field originally developed by Paul, Yoon and Smith (PYS)[41] and subsequently modified by Waheed et al.[33,35] In this model, CH_2 and CH_3 monomers are represented as united atom (UA) beads; chemical details of the alkane chain are otherwise fully maintained. The PYS model has been shown to reproduce important physical properties of the melt phase including dynamical properties and chain distributions. The melting temperature and enthalpy of fusion of the n-alkane rotator phase are accurately represented by this model.[37] Crystal transitions to orthorhombic (polyethylene) or monoclinic (n-alkane) phases are typically not captured by the PYS model as a consequence of its UA nature.

Simulations were performed using the LAMMPS molecular dynamics software package.[42] In LAMMPS, the convention for the dihedral angle is that $\varphi_{trans} = 180°$ which differs from the PYS forcefield, where the convention is $\varphi_{trans} = 0°$. This change of convention was implemented through a simple geometric transformation that does not affect the energy pre-factors for the dihedral potential. All results are presented for simulations in an NPT ensemble with pressure $P = 1$ atm. Pressure and temperature were maintained at their set point values using a Nosé-Hoover barostat and thermostat; the damping frequencies used were ω_P =1/(1000 fs) for the barostat and ω_T = 1/(10 fs) for the thermostat. The forces were integrated using the rRESPA multiple time step integrator, with the time step for the pairwise nonbonded force calculations set to 5 fs and the time step for all other force interactions (bond, angle, dihedral) set to 2.5 fs. The integration method allowed the use of a large time step for pairwise interaction

calculation while ensuring energy conservation by implementing more frequent intra-molecular interaction calculations. For all simulations, an orthorhombic simulation box was used, with all side lengths allowed to vary independently and periodic boundary conditions applied.

The simulations used to characterize the melting point T_m of n-pentacontane ($C_{50}H_{102}$ or C50) were performed on systems containing 288 C50 chains. The chains were initially arranged as fully extended chains in a pseudo-hexagonal packing with their chain axes parallel to the *y*-direction. Approximately 75 percent of the chains were melted to introduce a crystal-melt interface along the *xy* plane. Selective melting was achieved by manipulating the force field using a technique proposed by Bai et al.[43] and previously used by Yi and Rutledge.[37] The energy pre-factors for the bond stretch, angle bending, dihedral, and van der Waals interactions of the designated crystal phase were doubled to elevate the melting temperature artificially to T_m'. Amorphization of the unmodified chains was then achieved by increasing the temperature above T_m yet below T_m'. Upon formation of a flat crystal-amorphous interface, all chains were restored to the original force field parameters for subsequent simulation. Five molecular dynamics simulations were run at each of several temperatures between 365 and 375 K. From the increase ($T > T_m$) or decrease ($T < T_m$) in total crystallinity of the partially amorphized C50 with time, T_m was determined.

The simulated system used to characterize crystal growth and surface nucleation in C50 comprised two distinct components. The first component was the n-alkane phase, which consisted of 364 C50 chains, arranged identically to the initial system of crystalline C50 chains in our melting point simulations, 14 chains making up a single layer in the *xy* plane, and 26 layers in the *z*-direction. The second component was a crystalline polyethylene phase constructed solely of methylene sites and arranged initially in the conventional orthorhombic PE unit cell. Bonds between methylene groups along the chain axis in the chains of the polyethylene phase were continued across the periodic boundary in the *y*-direction, to create chains of infinite length. The chains were tilted by 9 degrees from the *y*-direction in the *xy* plane, so that crystal stem segments were not bonded with themselves through the periodic boundary condition.

Without this tilt, abnormally rapid diffusion along the chain axis was observed. The thickness of the PE phase in the *z*-direction was 1.6 nm, large enough to screen molecular interactions in the n-alkane phase on either side (Lennard-Jones cutoff distance = 1 nm). The initial dimensions of the simulation cell were 6.72 nm x 6.5 nm x 12.45 nm.

Amorphization of the C50 component was again achieved using the technique of Bai et al.[43] In the first step, the energy pre-factors for the bond stretch, angle bending, dihedral, and LJ interactions of the PE crystal phase were doubled to elevate artificially the melting temperature of the PE component while equilibrating the as-constructed crystal C50 at room temperature (300 K) for ~0.5 ns. Then, the temperature was increased to 500 K to induce melting of the C50 component, while maintaining a relatively rigid crystal PE phase. The simulation at 500 K was continued for 20 ns, the first 10 ns of which was sufficient to erase all memory of the original crystalline structure in C50. Complete transition to an amorphous state was confirmed by monitoring the relaxation of R_g from its fully extended conformation value to one compatible with a random coil. Additionally, the melt density was 0.76 g/cm^3, which is comparable to the melt density of similar n-alkanes at these temperatures.[44] The last 10 ns of the simulation at 500K was used to generate 20 independent configurations to serve as starting points for subsequent quenching and crystal growth simulations. Figure 2(a) illustrates a typical system after amorphization of the C50 component.

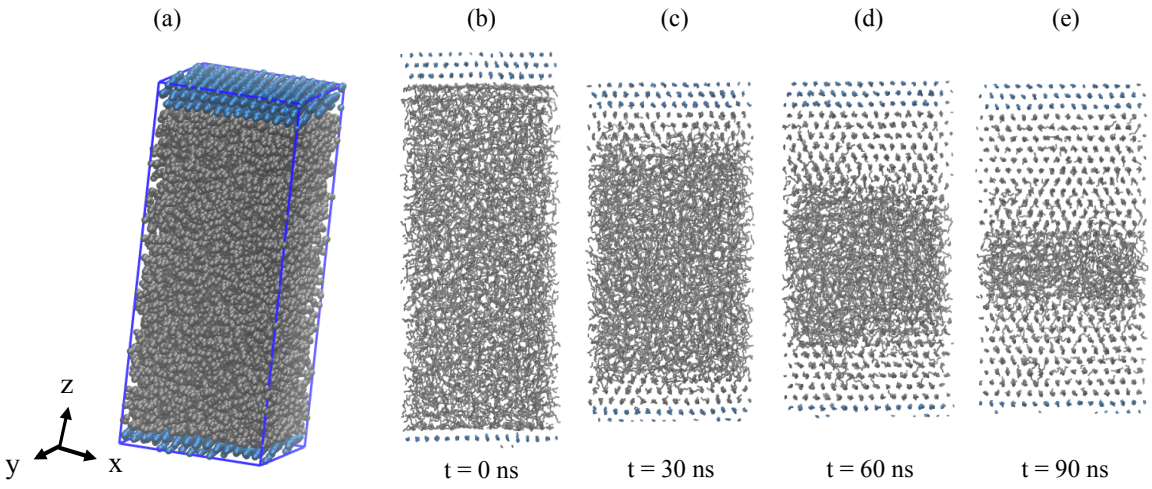

Figure 2 (a) Simulation box before the quench step; a crystalline PE phase (blue) alternates with an amorphous melt of C50 chains (grey). Snapshots from MD simulation viewed down the *y*-axis following a quench from 500K to 360 K after (b) 0 ns, (c) 30 ns, (d) 60 ns and (e) 90 ns of elapsed time.

Crystallization was induced by instantaneously quenching all 20 configurations to the desired crystallization temperature, T_c, and allowing the systems to evolve isothermally. Crystal growth was monitored through the use of a local p_2 order parameter. The order parameter $p_2(i)$ for UA bead i was defined as

$$p_2(i) = \left\langle \frac{3\cos^2\theta_{ij} - 1}{2} \right\rangle_j \tag{7}$$

where θ_{ij} is the angle between the vector spanning the midpoints of the bonds on either side of the i^{th} UA, and that spanning the bonds of the j^{th} UA. The average is taken over all of the j neighboring UAs that lie within a cutoff distance $r_{ij} < r_{p2}$ of the i^{th} UA bead. The value of r_{p2} was chosen to be 2.5σ, where σ is the Lennard-Jones interaction range parameter. This choice is consistent with previous crystallization studies of n-alkanes.[37,38] The $p_2(i)$ was averaged over the entire simulation cell in order to determine the total crystallinity in the simulations used to estimate T_m.

Surface clusters were identified within slices of material taken normal (*xy* plane) to the growth direction (*z*). The thickness of each slice was approximately equal to the thickness of a single layer of chain segments in the C50 crystal (0.4 nm). Slices were defined starting at the original PE crystal interface and continued into the bulk n-alkane phase along the *z*-direction. A clustering algorithm was used to identify crystalline clusters within a layer. Bead *j* was assigned to a cluster containing bead *i* if the following criteria were met: $p_2(j) > 0.4$, $r_{ij} < 1.3\sigma$ and beads *i* and *j* belong to the same slice. The first two criteria are consistent with those used by Yi et al to aggregate crystal sites into clusters in homogeneous nucleation studies.[37,38] The third criterion is particular to the analysis for surface nucleation. The number of crystalline beads $N_c(z)$ in a given slice was also identified as a function of time from this clustering algorithm. The number of crystalline beads scaled by the total number of beads in a given slice N_T gives the fractional crystallinity of a layer, $X(z) = N_c(z)/N_T$.

For a given simulation trajectory, the fractional crystallinity $X(z)$ versus the surface normal direction (z) was used to identify the location of the crystal-amorphous interface. Adapting the Gibbs dividing surface technique employed by Hutter et al,[45] the gradual transition in X(z) from crystal to amorphous melt was approximated by a step function at $z = D$. The Gibbs dividing surface was chosen such that the integral of the difference between the true crystallinity profile and the step function approximation vanishes when the step function is located at $z=D$:

$$\Delta X_{c,\mathrm{int}} = \int_{-\infty}^{\infty} \left[X^{step}(z \mid D) - X(z) \right] dz = 0 \qquad (8)$$

Scaling X(z) to vary between $X_{-\infty}$ and $X_{+\infty}$, the values of fractional crystallinity observed far removed from the interface on either side, $X'(z) = \left(X(z) - X_{-\infty}\right) / \left(X_{+\infty} - X_{-\infty}\right)$, Eq. (8) can be written:

$$\Delta X'_{c,\mathrm{int}} = \int_{-\infty}^{\infty} \left[H(z-D) - X'(z) \right] dz = 0 \qquad (9)$$

where $H(x)$ is the Heaviside step function. Using the position of the PE surface as reference (z=0), the value of D was used to measure the displacement of the interface within a given trajectory. Twenty replicate simulations having two interfaces per simulation cell provided a total of 40 measurements of the growth rate $G=|dD/dt|$ at each temperature.

For each simulation, nucleation and spreading was tracked in the first 9 layers adjacent to each interface. Even when the crystal growth front reached the ninth layer, the remaining amorphous region at the center of the simulation was still at least 4 nm wide. Based on a radius of gyration of < 2 nm for C50, this width should be sufficient to ensure that the two growth fronts in each simulation were independent of each other for the layers analyzed. Measurement of the average local p_2 order parameter near the midpoint between the two interfaces at the end of the simulation further confirmed that an amorphous region of width Δz = 2 nm remained, indicated by $p_2(z) \sim 0$.

5. Results

From the C50 simulations used to find T_m, the total crystallinity as measured by P_2, the global average of the local order parameter $p_2(i)$, was plotted as a function of time for each temperature of study. An increase in P_2 with time signifies that the temperature of the simulation was lower than the melting temperature predicted by the force field, while a decrease in P_2 with time indicates the opposite. Figure 3 shows that at 365 K, the order parameter increased, whereas at 375 K it decreased. At 370 and 372 K, the order parameter hardly changed in 20 ns of simulation. Thus we determined the melting temperature T_m for n-pentacontane using the PYS forcefield to be 370 ± 5 K. This compares favorably with the experimentally reported temperature, T_m = 367 K.[46]

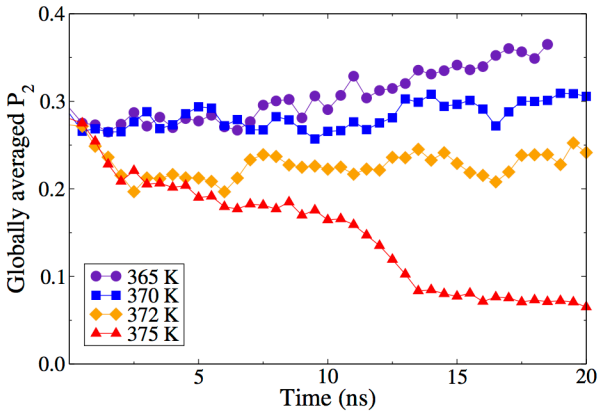

Figure 3. Global order parameter, P_2, as a function of time at four different temperatures for a system of 288 C50 chains. The equilibrium melting point is $T_m = 370 \pm 5$ K.

Having determined the melting temperature for C50, temperatures ranging from 300 to 370 K were chosen for quenching and subsequent examination of crystal growth in the 2-component (PE/C50) system. Figure 4 summarizes the results for growth front propagation at 300, 320, 340, 360 and 370 K. Within each simulation trajectory, growth occurs at two interfaces, due to the periodicity of the system. Figure 4(a) is a representative example of the $X(z)$ profiles obtained for one trajectory at 360 K at different simulation times, showing propagation from a single interface. Growth front propagation at 340 K and above was relatively rapid. The growth front proceeded inward smoothly from each interface over the course of a simulation, producing high order ($X(z) > 0.9$) on the crystal side. The $X(z)$ profiles at the lower temperatures of 320 and 300 K were noticeably rougher, and growth rates much slower. Observations of the system at long times revealed that crystallites contained chains in a fully extended state.

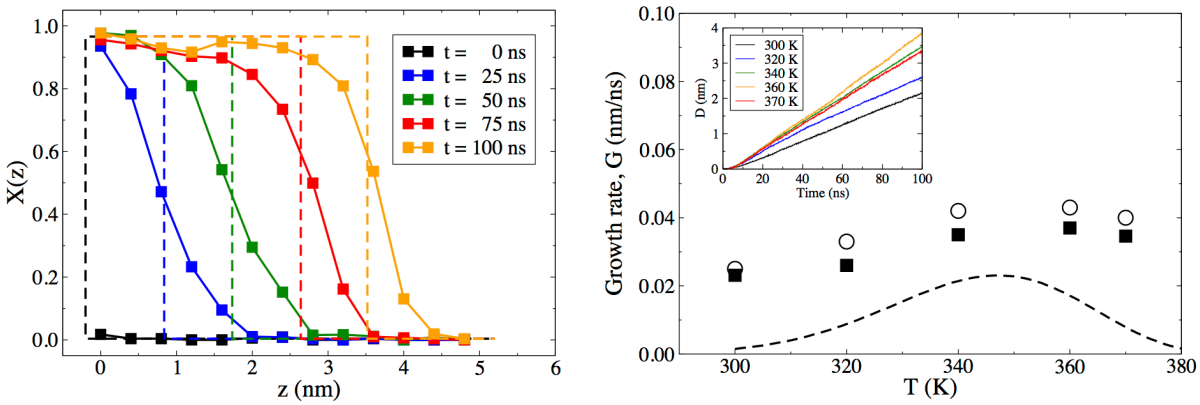

Figure 4. (a) $X(z)$ profile in simulation box at 0, 25, 50, 75 and 100 ns following quench to 360 K. Dashed lines show the profile using a step approximation, with the Gibbs dividing surface located at $z = D$. (b) Growth front propagation rate, G, as a function of temperature (filled symbols), obtained from the location of the Gibbs dividing surface at D (inset). Also shown are the growth rates obtained from waiting times (open symbols). The growth rates reported for C50 by of Waheed et al[33] are included as the dashed curve. Results were averaged over all trajectories for temperatures ranging from 300-370 K.

The temperature dependence of the growth rate is shown in Figure 4(b), and the average displacement D versus time at each temperature is shown in the inset. The growth rate was obtained from the slope of D versus time in the region of linear growth ($1 < D(t) < 2$ nm). A maximum in growth rate with temperature was observed, which is consistent with empirical observations.[1] Such a maximum in the growth rate is expected between the glass transition temperature T_g and the melting temperature T_m. As T_c approaches T_g from above, molecular mobility is impeded, slowing diffusive transport to the growing crystal front. Conversely, as T_c approaches T_m from below, the thermodynamic driving force for nucleation decreases. The competing processes result in a temperature at which the crystal growth rate is maximal. In our study, this temperature was around 360K.

In their earlier studies, Waheed et al. presented a model for the crystal growth rate.[33] The model was parameterized using simulation data for the crystallization of C20, C50, and C100 chains. While the

general temperature dependence and the temperature at which the maximum crystallization rate occurs are qualitatively similar to our results, the simulations of Waheed underestimated the crystallization rate observed here by at least a factor of two for all temperatures studied. The discrepancy likely arises from differences in the size of the simulation cell used in the two works. In the simulations of Waheed et al, the simulation box was large enough to accommodate a fully extended C50 chain and to observe crystal growth over several layers, but the third dimension in which spreading occurs was less than half that used in this study (2.59 nm vs 6.72 nm). We speculate that finite size effects arising from impingement of the spreading nucleus with itself in this third dimension was responsible for the reduction in growth rate observed, as the chains must disengage within a narrow zone to complete crystallization within a layer. Although the *x*-dimension in this work was larger, it too was finite; thus the predicted growth rates in this work should be viewed as lower bounds on the true crystal growth rates in C50. Modest finite size effects were confirmed by running simulations using both larger and smaller boxes. Growth rates increased by ~10% upon doubling the *x*-dimension, and decreased by a similar amount upon halving the *x*-dimension; these shifts are consistent with the explanation given here.

Figure 5(a) shows the temporal evolution of the number of crystalline beads N_c within each of the first 4 layers adjacent to the PE surface in a typical trajectory at 360 K. The number of crystalline beads is further divided into the individual contributions of the 5 largest clusters in each layer. It is readily apparent that crystallization within a layer was dominated by the largest cluster at this temperature. For all simulation trajectories, the first layer showed a nearly spontaneous increase in cluster size, and the cluster in this layer continued to spread until it reached the size of a fully crystallized layer (N_T=700 UA beads). Crystallization in subsequent layers (e.g. layers 3 and 4) was shifted towards later times, due to the time required for propagation of the growth front from the PE surface (at time zero) to these more distant layers. Figure 5(b) shows the evolution of N_c in a typical trajectory at 320 K. At this lower temperature, the second largest cluster was more prominent, indicative of multiple surface nucleation events within a

layer. In some cases, it appears as though two independent nucleation events occurred, resulting in surface nuclei that grew, and eventually merged, into a single nucleus.

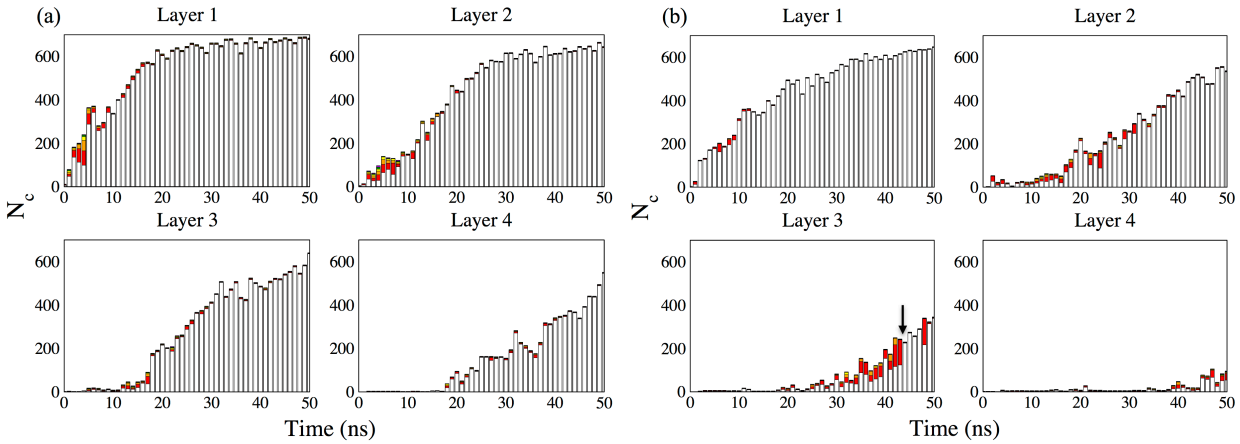

Figure 5. Size distribution of surface clusters in layers 1-4 of a sample trajectory at 360K (a) and 320K (b). The stacked height of each bar is the total number of crystalline beads, N_c. Subdivisions in the bar represent the size of the 1st (grey), 2nd (red), 3rd (orange), 4th (yellow), and 5th (green) largest clusters in a layer, in descending order. The histogram of grey bars is equivalent to a plot of n_{max} vs time for each layer; the colored bars convey the relative importance of multiple nucleation events; except perhaps for the lowest temperature, multiple nucleation appears to have been relatively unimportant in this work. The arrow in Figure 5(b) highlights a merging event in layer 3 at 45 ns.

The value of α for the spreading term, $\tau_s(n_{max})$, Eq. (5), was determined from the shape evolution of the largest cluster n_{max} in a layer. For this purpose, the number of crystalline stems n_{stems} within the largest cluster in any given layer was recorded over the course of each simulation and plotted versus the total size of the cluster, n_{max}; Figure 6 shows one case for T_c = 360 K. A relationship of the following form is expected,

$$n_{stems} = C\left(n_{\max}\right)^{\alpha} \tag{10}$$

where C is a pre-factor for the power-law relationship and α is the scaling exponent. Up to about n_{max} = 300, the number of crystalline stems within the cluster increased with the size of the cluster, as expected. Beyond n_{max} = 300, n_{stems} leveled off, due to impingement of the nucleus with its periodic image. From the log-log plot of n_{stems} versus n_{max} up to n_{max} = 300, we determined the value α = 0.6 at 360 K, indicative of nearly isotropic spreading. Similar values of α were obtained at all other temperatures as well. Examination of Figure 6 shows that α = 1 (linear spreading by addition of full stems) can be excluded. For purposes of MFPT analysis, α = 1/2 (isotropic spreading) was assumed.

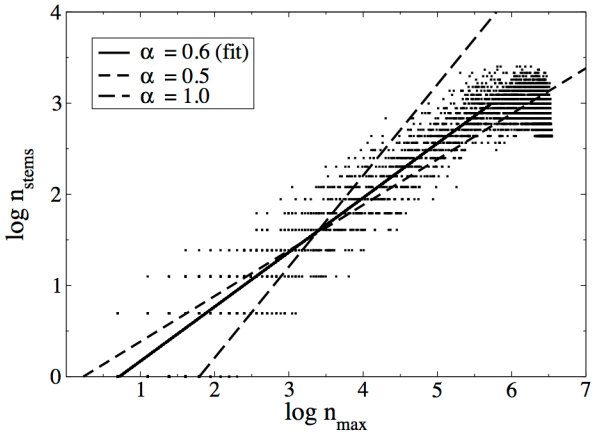

Figure 6. Log-log plot of the number of crystal stems n_{stems} within the largest cluster versus the size of the largest cluster n_{max}, for a typical trajectory at 360 K. Data points are shown for the largest clusters within each layer at numerous time points. A best-fit linear relationship for nuclei below 300 UA beads in size is included. For comparison, lines of slope 1 and ½ are also shown.

Figure 7 shows the MFPT results for the largest cluster n_{max}, up to n_{max} = 300, in each of the first 9 layers near a PE surface at 360 K. As evidenced by their short MFPT, small clusters up to n_{max} = 15 were rapidly sampled for all layers k, indicative of the thermal population of small clusters in the melt. A waiting

period was observed before the appearance of clusters of $n_{max} > 30$, indicated by a sharp increase in MFPT for $15 < n_{max} < 30$. The magnitude of the waiting period was proportional to the layer number k. Each layer exhibited continued increase in MFPT for $n_{max} > 30$, indicative of finite, lateral spreading within a layer. The MFPT model with isotropic spreading was fit to the raw MFPT curves, as shown in Figure 7. In the first layer, clusters of large n_{max} were reached too quickly to be resolved by the sampling frequency employed (0.2 ns), but in any case were not important for characterizing crystal growth in C50. For the other layers, the model describes the data reasonably well.

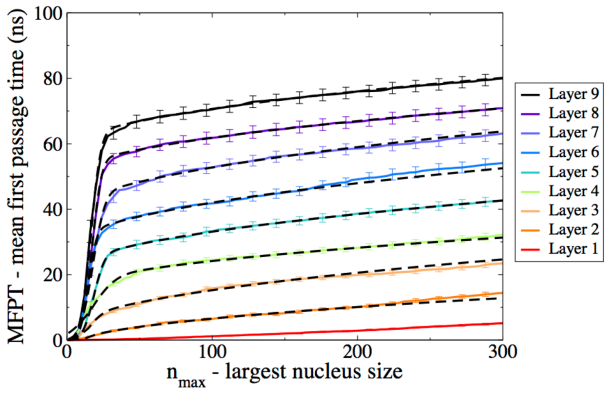

Figure 7. MFPT of the largest cluster for each of the first 9 layers from the PE crystal surface, after quenching to 360 K. Data (solid lines) were fit to a MFPT model (dashed lines) for n_{max} up to 300 UA; larger values of n_{max} exhibited evidence of finite size effects, since the layer was more than 40% crystallized at that point. Layers nucleate and spread sequentially in time; thus the lowest curve represents layer 1 (closest to the PE surface) and the highest curve represents layer 9.

From the MFPT curves for layers 2-9 at each temperature, values for the waiting time τ^*, the size of the critical surface nucleus n^*, the Zeldovich factor Z, and the spreading rate s, were obtained. The values for $n^* = 20 \pm 5$ and $Z = 0.06 \pm 0.02$ were found to be relatively insensitive to temperature or layer number (beyond layer 2). The results for s and τ^* are plotted as functions of layer number for each temperature in Figure 8. The surface spreading rate decreased considerably with increasing layer number k, and leveled

off beyond layer 3, approximately. The faster spreading rates observed for low layer numbers are indicative of the influence of the PE crystal, while the values observed for high layer numbers should be representative of crystal growth in C50. We therefore distinguish between "near surface" behavior during crystallization, which includes the first nanometer (approximately 3 layers) near the PE/C50 surface where the foreign influence of the PE surface is significant, and "far from surface" behavior, which should be representative of crystal growth in neat C50. "Far from surface" behavior persists for several layers in the bulk C50 phase during growth front propagation. In each of these layers, a surface of crystallized C50 chains was created dynamically, which then served as the surface upon which the next layer nucleated and spread. Depending on the mechanism of growth, a more-or-less steady process of surface nucleation and spreading continued from layer to layer, resulting in progression of the growth front. The spreading rate s decreased with temperature for $T_c < 360$ K.

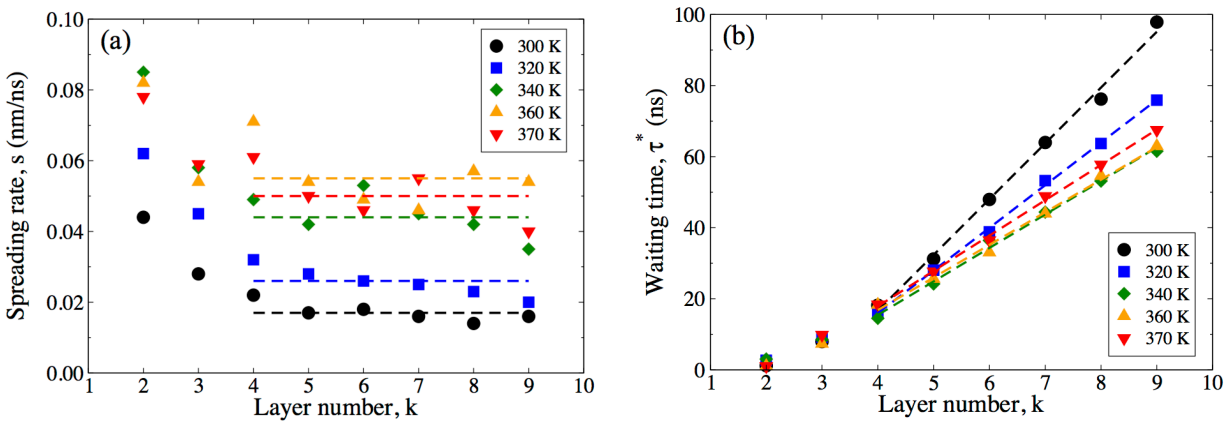

Figure 8. (a) Lateral spreading rate s versus layer number k for each crystallization temperature. (b) Waiting time τ^* versus layer number, for each temperature. The plotted values are the parameters of the MFPT model that best fit the raw data, according to least sum of squared deviations. The average spreading rate in the "far from surface" region at each temperature is highlighted by the dashed lines in (a), and a linear fit for the "far from surface" region is shown by the dashed lines in (b).

As expected, the waiting time τ^* increased with layer number k. $\Delta\tau^*$ between layers was multiplied by the layer thickness (0.4 nm) to obtain a second estimate of the growth rate G. This alternative estimate of G is shown in Figure 4(b); its temperature dependence mimics that of the growth rate estimated from the displacement of the Gibbs dividing surface, including the maximum near 360 K. However, the magnitude of the growth rate based on waiting times is systematically higher than that based on the order parameter, by as much as 20%. We have traced this difference in the predicted growth rate G back to finite size effects that impact the two methods of growth rate determination differently. In general, finite x- and y-dimensions inhibited spreading in the xy plane, which translated to an overall reduced crystal growth rate from what would be observed in an unhindered system. The reduction in the spreading rate due to impingement was more pronounced at higher crystallinities in a given layer; a considerably longer reorganization time was required to achieve 75% - 100% crystallinity within a layer as the disengagement zone for chains continued to narrow. The growth rate measured by the tracking the location of the Gibbs dividing surface is essentially a metric for the time to reach 50% crystallinity within a layer, whereas the estimation of growth rate from waiting times refers to the time to reach ~3% crystallinity. The discrepancy in growth rates therefore indicates that the passage time from 3% to 50% crystallinity is also increased by impingement in the lateral direction. Rigorously, this dependence of growth rate on percentage of crystallinity within a layer suggests our systems still had not quite reached steady-state, where one should obtain the same growth rate, regardless of percentage of crystallinity used to measure it. Thus we believe the growth rates determined from waiting times are even better lower bound estimates of the crystal growth rate in C50 than those determined from the propagation of the p_2 order parameter profile, as they should be less impacted by finite size effects.

Figure 9 shows the surface nucleation rate i as a function of the isothermal crystallization temperature T_c. For each simulation trajectory, the waiting times used as the bounds of integration in Eq. (6) were obtained from the MFPT analysis. The crystalline area recorded for all layers $A_k(t)$ was subsequently passed to Eq. (6) to estimate the corresponding surface nucleation rate upon each layer of crystallized

C50. The surface nucleation rate as a function of layer number *k,* averaged over all replicate trajectories, is shown in the inset of Figure 9. The nucleation rate was observed to be independent of layer number in the "far from surface" region, $k \geq 4$. This average surface nucleation rate in the "far from surface" region is plotted in Figure 9. Surface nucleation rates were found to be about 0.05 $nm^{-2}ns^{-1}$, and to vary little with temperature. This lack of a strong temperature dependence suggests that the activation barrier for surface nucleation is comparable to or smaller than the thermal energy, kT, if it exists at all.

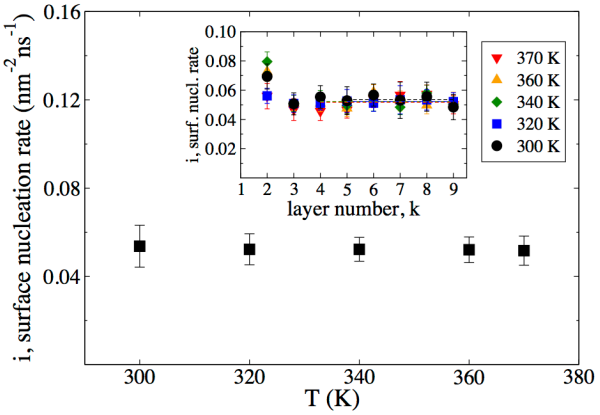

Figure 9. Surface nucleation rate *i* at the crystallization growth front in C50 as a function of isothermal crystallization temperature T_c. The reported rates are an average of the surface nucleation rates in the "far from surface" regime (inset).

6. Discussion

By means of the foregoing analysis of molecular dynamics simulations, we have determined the crystal growth rate for C50 to be about two times higher than previously estimated, but qualitatively similar in its temperature dependence. Using a MFPT analysis, we have also estimated surface nucleation rates, critical surface nucleus sizes and surface spreading rates of each of the first nine molecular layers near a pre-existing PE crystal surface, for the first time. In so doing, we can distinguish between these properties for layers that are within 1.0-1.2 nm of the PE surface (layers 1-3) and those that are farther away (layers 4-

9). The first several layers exhibit behavior that would be typical of heterogeneous crystallization on a foreign surface, whereas the latter layers are self-similar and representative of crystal growth in the C50 melt. We have additionally determined the temperature dependences of these properties for crystal growth in the C50 melt.

The critical surface nucleus was found to be about 20 UA beads, smaller than a single chain of C50, and involved more than one chain. By analyzing *trans* torsional states in the polymer chains at the crystal growth front, Waheed observed a jump from 10 or fewer UA beads to 20 beads, indicating a nucleation transition. In this study, after attaining a cluster size of 20 UA beads, the nucleus quickly evolved to larger sizes and spread nearly isotropically across the surface. These two observations contradict the usual interpretation of LH theory, which stipulates that the critical nucleus is a fully-extended crystal stem, and that spreading occurs laterally from this stem. The geometry of the critical surface nucleus compares favorably with observations by inspection of surface ordering carried out by Waheed et al.[33] and with predictions by Wagner and Phillips,[47] where it was estimated that such nuclei consist of 3-5 stems. Waheed estimated these stems to be approximately 20 UA beads long; however, the more quantitative analysis employed here indicates the stems in the critical surface nucleus to be around 5 UA on average. Growth of the cluster within a layer occurs via stem lengthening as well as by addition of new stems or monomers to the lateral edges of the cluster. The small size of the critical surface nucleus suggests a small free energy barrier to surface nucleation. In homogeneous nucleation, the critical nucleus size was found to be on the order of 150 UA beads, albeit at a relatively deep (30%) supercooling.[32] Supercooling was much shallower in this study, between 2-20%, and the critical nucleus size was around 20 UA beads for all cases. The difference in critical nucleus sizes is consistent with a much lower activation energy for surface nucleation than for primary (homogenous) nucleation.

The surface roughness at the growth front is known to vary with supercooling ΔT for crystallizing polymers.[20] As the depth of supercooling increases, the growth front is believed to become more and more “rough”, attributed to the increasingly prolific formation of smaller and smaller surface nuclei,

while remaining macroscopically faceted.[20,48] This phenomenon has been called "kinetic roughening". On the other hand, at higher temperatures (shallow undercooling), it has also been argued that the growth surface can become rougher due to enhanced fluctuations of entropic origin, a "thermodynamic roughening", and that such fluctuations indicate the disappearance of the barrier to surface nucleation and give rise to macroscopically curved growth fronts.[20,48] Thus, the roughness R of the interface between the crystal and melt and its dependence on temperature could provide useful insights into the mechanism of growth and the relative rates of surface nucleation and spreading. The squared roughness R^2 was evaluated at any instant in time using the analogue of Eq. (9) that computes the distance-weighted deviation of the growth front from its mean position, as follows:

$$R^2 = \int_{-\infty}^{\infty} \left[H(z-D) - X'(z) \right] (z-D) dz \qquad (11)$$

The instantaneous surface roughness determined by Eq. (11) at 300, 320, 340, 360 and 370 K for crystallizing *n*-pentacontane is given in Figure 10. The surface roughness increases with distance from the crystalline PE substrate at all crystallization temperatures T_c. It appears that the roughness approaches an asymptotic, equilibrium value within about 60 ns at 300 K, but such asymptotic values are not reached within the 100 ns of simulation time at the higher temperatures. For all temperatures, $R/h > 1$ at long times, which indicates that more than a single layer is actively crystallizing at the growth front over the entire range of temperatures. Nevertheless, it would appear that roughness is not simply a monotonically increasing function of supercooling, and that there may even be a maximum roughness at some intermediate temperature (e.g. 320-340 K). The current results are only preliminary, but they do suggest that the description given above is incomplete, and that a careful and more quantitative interpretation of roughness in terms of the temperature dependence of surface nucleation and spreading rates is warranted.

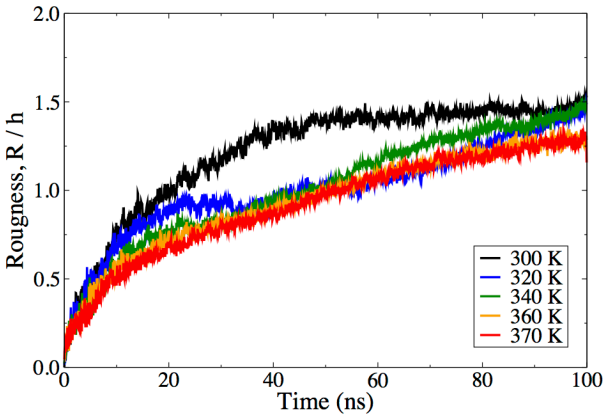

Figure 10. Surface roughness at the crystal growth front for C50 scaled by the thickness of a layer h = 0.4 nm, as a function of isothermal crystallization temperature T_c.

7. Conclusions

We have reported a method to quantify surface nucleation events and subsequent spreading at the crystal growth front from molecular dynamics simulations. A mean first passage time analysis was applied to the evolution of the largest 2-dimensional cluster within layers in the vicinity of the crystal growth front for a supercooled C50 melt. From this, we determined critical surface nucleus sizes, waiting times, and ultimately surface nucleation rates. Lateral spreading rates were found to be temperature-dependent, with a maximum near 360 K for C50, while surface nucleation rates were found to be temperature-independent, contrary to expectation.

Following nucleation, surface nuclei were observed to spread isotropically, based upon the ratio of number of stems to the number of beads within a crystal nucleus. The spreading rates for post-critical nuclei were estimated using an isotropic spreading model and were found to increase with temperature, as expected. Estimates of the surface nucleation rates were obtained by two methods, using waiting times for the nucleation of each layer and also the layer crystallinity as a function of time, and were found to be in reasonable agreement. Finite size effects during simulation were mitigated, but not completely eliminated. In contrast to the usual interpretation of LH theory, we found a roughly circular nucleus with

approximately 20 UA beads formed, which then spread isotropically across the surface. The roughness of the interface at the growth front is found to be temperature-dependent, but apparently not in a manner consistent with conventional wisdom.

The growth rates, surface spreading rates and surface nucleation rates obtained in this work provide a foundation for further study of surface nucleation in polymer systems by molecular simulation. The techniques developed here can be applied beyond surface nucleation during growth of n-alkanes to nucleation induced by heterogeneous surfaces of additives in polymer melts. In a companion paper[49], the results are used directly to parameterize a crystal growth kinetic model that can be applied to arbitrarily large systems and long times.

8. References

(1) Ziabicki, A. *Fundamentals of Fibre Formation*; Wiley: London, UK, 1976; pp 75-147.

(2) van Krevelen, D. W. Crystallinity of polymers and means to influence crystallization process, *Chimia*, **1978**, 32 279-294.

(3) Keller, A. A note on single crystals in polymers: evidence for a folded chain configuration, *Philos. Mag.*, **1957**, 2 1171-1175.

(4) Keller, A. The morphology of crystalline polymers, *Macromol. Chem. Phys.*, **1959**, 34, 1-28.

(5) Carraher, C. E.; Seymour, R. B. *Polymer Chemistry*; CRC Press: Boca Raton, Florida, 2003; pp 44–45.

(6) Mandelkern, L. The crystallization of flexible polymers, *Chem. Rev*. **1956**, 56, 903-958.

(7) Mandelkern, L. *Crystallization of Polymers: Vol. 2, Kinetics and Mechanisms*; Cambridge University Press: Cambridge, UK, 2004; pp 357-408.

(8) Bassett, D. C.; Keith, H. D. Electron microscopy and spherulitic organization in polymers, *Crit. Rev. Solid State Mater. Sci.*, **1984**, 12, 97-163.

(9) Toda, A.; Okamura, M.; Taguchi, K.; Hikosaka, M.; Kajioka, H. Branching and higher order structure in banded polyethylene spherulites, *Macromolecules*, **2008**, 41, 2484-2493.

(10) Muthukumar, M. Commentary on theories of polymer crystallization, *Eur. Phys. J. E*, **2000**, 3,199-202.

(11) In the polymer literature, LH theory is sometimes referred to as a "secondary nucleation" theory, to contrast it with primary nucleation of a crystal phase from the melt. In this context, "secondary nucleation" refers specifically to the formation of a nucleus on the surface of a pre-existing crystallite. However, in the broader literature on crystallization, secondary nucleation is also used to describe breakup of a primary, or parent, nucleus into secondary, or daughter, nuclei as the result of collisions or mechanical forces, where such secondary, or "second generation" nuclei continue to grow into mature crystallites (c.f. Melia, T. P.; Moffitt, W. P. *Ind. Eng. Chem. Fund.* **1964**, 3, 313; Ottens, E. P. K.; de Jong, E. J. *Ind. Eng. Chem. Fund.* **1973**, 12, 179.) To avoid such confusion, we employ the term "surface nucleation", as originally used by Lauritzen and Hoffman, 1960, throughout this paper to mean the same thing as "secondary nucleation".

(12) Lauritzen, J. I.; Hoffman, J. D. Theory of formation of single polymer crystals with folded chains in dilute solution, *J. Res. Nat. Bur. Std. A*, **1960**, 64, 73.

(13) Hoffman, J. D.; Frolen, L. J.; Ross, G. S.; Lauritzen, J. I. On the growth rate of spherulites and axialites from the melt in polyethylene fractions: regime I and regime II crystallization, *J. Res. Nat. Bur. Std. A,* **1975,** 79A, 671.

(14) Hoffman, J. D.; Miller, R. L. Kinetics of crystallization from the melt and chain folding in polyethylene fractions revisited: theory and experiment, *Polymer*, **1997**, 38, 3151-3212.

(15) Armisted, J. P.; Hoffman, J. D. Direct evidence of regimes I, II, and III in linear polyethylene fractions as revealed by spherulite growth rates, *Macromolecules*, **2002**, 35, 3895-3913.

(16) Cheng, S. Z. D.; Janimak, J. J. Crystal growth of intermediate-molecular-mass poly(ethylene oxide) fractions from the melt, *Polymer*, **1990**, 31, 1018.

(17) Cheng, S. Z. D.; Janimak, J.J.; Zhang, A.; Chang, H. N. Regime transitions in fractions of isotactic polypropylene, *Macromolecules*, **1990**, 23, 298-303.

(18) Frank, F.C.; Tosi, M. On the theory of polymer crystallization, *Proc. R. Soc. Lond A*, **1961,** 263, 323-339.

(19) Point, J. J. A new theoretical approach of the secondary nucleation at high supercooling, *Macromolecules*, **1979**, 12, 770-775.

(20) Armistead, K.; Goldbeck-Wood, G.; Keller, A. Polymer crystallization theories, *Adv. Polym. Sci,* **1992**, 100, 219-312.

(21) Sadler, D.M.; Gilmer, G.H. A model for chain folding in polymer crystals: rough growth faces are consistent with the observed growth rates, *Polymer*, **1984**, 25, 1446-1452.

(22) Doye, J. P. K.; Frenkel, D. Kinetic Monte Carlo simulations of the growth of polymer crystals, *J. Chem. Phys.*, **1998**, 110, 2692-2702.

(23) Binsbergen, F. L. A revision of some concepts in nucleation theory, *Colloid Polym. Sci.*, **1970**, 237, 289-297.

(24) Rastogi, R.; Hikosaka, M.; Kawabata, H.; Keller, A. Role of mobile phases in the crystallization of polyethylene; metastability and lateral growth, *Macromolecules*, **1991**, 24, 6384-6391.

(25) Keller, A.; Hikosaka, A.; Rastogi, S.; Toda, A.; Barham, J.; Goldbeck-Wood, G. An approach to the formation and growth of new phases with application to polymer crystallization: effect of finite size, metastability, and Ostwald's rule of stages, *J. Mater. Sci.*, **1994**, 29, 2579-2604.

(26) Strobl, G. From the melt via mesomorphic and granular crystalline layers to lamellar crystallites: a major route followed in polymer crystallization, *Eur. Phys. J. E*, **2000**, 3, 165-183.

(27) Talanquer, V.; Oxtoby, D. W. Crystal nucleation in the presence of a metastable critical point, *J. Chem. Phys.*, **1998**, 109, 223-227.

(28) Pan, W.; Kolomeisky, A. B.; Vekilov, P. G. Nucleation of order solid phases of proteins via a disordered high-density state: phenomenological approach, *J. Chem. Phys.*, **2005**, 122, 174905.

(29) Kashchiev, D.; Vekilov, P. G.; Kolomeisky, A. B. Kinetics of two-step nucleation of crystals, *J. Chem. Phys.*, **2005**, 122, 244706.

(30) Meyer, H.; Müller-Plathe, F. Formation of chain-folded structures in supercooled polymer melts examined by MD simulation, *Macromolecules*, **2002**, 35, 1241-1252.

(31) Lavine, M.S.; Waheed, N.; Rutledge, G. C. Molecular dynamics simulation of orientation and crystallization of polyethylene during uniaxial extension, *Polymer*, **2003**, 44, 1771-1779.

(32) Yi, P.; Locker, C. R.; Rutledge, G. C. Molecular dynamics simulation of homogeneous crystal nucleation in polyethylene, *Macromolecules*, **2013**, 46, 4723-4733.

(33) Waheed, N.; Ko, M. J.; Rutledge, G. C. Molecular simulation of crystal growth in long alkanes, *Polymer*, **2005**, 46, 8689-8702.

(34) Shimizu, T.; Yamamoto, T. Melting and crystallization in thin film of n-alkane: a molecular dynamics simulation, *J. Chem. Phys.*, **2000**, 113, 3351-3359.

(35) Waheed, N.; Lavine, M. S.; Rutledge, G. C. Molecular simulation of crystal growth in n-eicosane, *J. Chem. Phys.*, **2002**, 116, 2301-2309.

(36) Hu, W.; Cai, T. Regime transitions of polymer crystal growth rates: molecular simulations and interpretations beyond Lauritzen-Hoffman model, *Macromolecules*, **2008**, 41, 2049-2061.

(37) Yi, P.; Rutledge, G. C. Molecular simulation of crystal nucleation in n-octane melts, *J. Chem. Phys.*, **2009**, 131, 134902.

(38) Yi, P.; Rutledge, G. C. Molecular simulation of bundle-like crystal nucleation from n-eicosane melts, *J. Chem. Phys.*, **2011**, 135, 024903.

(39) Milner, S. T.; Howard, M. P. A simple model for heterogeneous nucleation of isotactic polypropylene, *Macromolecules*, **2013**, 46, 6593-6599.

(40) Wedekind, J.; Strey, R.; Reguera, D. New method to analyze simulations of activated processes, *J. Chem. Phys.*, **2007**, 126, 134103.

(41) Paul, W.; Yoon, D. Y.; Smith, G. D. An optimized united atom model for simulations of polyethylene melts, *J. Chem. Phys.*, **1994**, 103, 1702-1709.

(42) Plimpton, S. Fast parallel algorithms for short-range molecular dynamics, *J. Comp. Phys.*, **1995**, 117, 1-19.

(43) Bai, X.; Li, M. Calculation of solid-liquid interfacial free energy: a classical nucleation theory based approach, *J. Chem. Phys*., **2006**, 124, 124707.

(44) Harmandaris, V. A.; Mavrantzas, V. G.; Theodorou, D. N.; Kroger, M.; Ramirez, J.; Ottinger, H. C.; Vlasssopoulos, D. Crossover from the rouse to the entangled polymer melt regime: signals from long, detailed

atomistic molecular dynamics simulations, supported by rheological experiments, *Macromolecules*, **2003**, 36, 1376-1387.

(45) Hutter, M.; in't Veld, P. J.; Rutledge, G. C. Polyethylene {201} crystal surface: interface stresses and thermodynamics, *Polymer*, **2006**, 47, 5494-5504.

(46) CSID:73140, http://www.chemspider.com/Chemical-Structure.73140.html (accessed 15:10, Oct 23, 2014).

(47) Wagner, J.; Phillips, P. J. The mechanism of crystallization of linear polyethylene, and its copolymers with octane, over a wide range of supercoolings, *Polymer*, **2001**, 42, 8999-9013.

(48) Schultz, J. M. *Polymer crystallization, the development of crystalline order in thermoplastic polymers*, Oxford University Press: New York, NY, 2001

(49) Bourque, A.; Rutledge, G. C. Kinetic model for layered growth during polymer crystallization, (in preparation).